International Forum on Aeroelasticity and Structural Dynamics
IFASD 2024
17-21 June 2024, The Hague, The Netherlands

# IMU-BASED DEFORMATION RECONSTRUCTION FOR HIGHLY FLEXIBLE WINGS

**Yuhui Zhang, Changchuan Xie* and Yang Meng**

Beihang University
Xueyuan Road 37, 100191 Beijing, China
zy2205331@buaa.edu.cn
xiechangc@buaa.edu.cn
summy@buaa.edu.cn

**Keywords:** Highly flexible wing, deformation reconstruction, inertial measurement unit

**Abstract:** This study presents a deformation reconstruction method for highly flexible wings based on distributed inertial measurement units (IMUs). According to coordinate transformation theory and kinematic formulas, the wing position and attitude equations were derived and wing deformation is obtained through angular velocity and acceleration collected by distributed IMUs. The developed technology will be applied to highly flexible flying wing model, where IMUs are connected to the surface of the wing beam. When the wing is subjected to directional dynamic loads, use the proposed method to calculate wing deformation. Meanwhile, finite element analysis (FEA) is conducted to verify the reconstructed wing deformation. The reconstruction results obtained by the proposed method are in good agreement with the FEA results.

## 1 INTRODUCTION

The wings of high aspect ratio are typically highly flexible, resulting in significant elastic deformations during flight [1]. The aerodynamic shape of the aircraft undergoes substantial changes, reflecting pronounced geometric nonlinearity in deformation characteristics [2]. The wing deformation of the solar powered drone Helios during level flight can reach 20% of its half span length. Such extensive deformations render traditional aeroelastic analysis methods, based on the assumption of small deformations, inapplicable. Therefore, there is a need for nonlinear analysis methods to enable real-time monitoring of large wing deformations.

The commonly used methods for measuring structural deformation are camera measurement and strain displacement measurement. Oliver [3] deployed four cameras in a wind tunnel to monitor blade deformation. Wei [4] proposed a non-contact three-dimensional full field deformation measurement scheme for wings under a large angle camera field of view for large single wing aircraft. Yuan [5] applied KO displacement theory to reconstruct the structural deformation of a beam wing and verified the feasibility and reliability of this method. Tessler [6] proposed the inverse finite element method, which uses the weighted least squares variational principle to describe the strain field and is applied to the structural deformation monitoring of spacecraft.

In recent years, the application of inertial measurement units in real-time measurement of wing deformation has received attention due to their advantages of low cost, small size, and high

accuracy. Leandro [7] proposed a rate gyroscope wing shape estimation (RG-WSE) method, which uses IMUs assisted by camera measurements for wing deformation measurement. Ali [8] conducted experimental verification on the wing model constructed using the RG-WSE method. Zhang [9] proposed an algorithm for wing elastic deformation based on distributed inertial measurement units and verified its effectiveness. Zhang [10] established an inertial network system and used a multi-sensor data fusion method to solve the problem of wing deformation. However, there is currently no relatively complete deformation measurement method for large flexible wings based on IMU.

This paper proposes a wing deformation reconstruction method based on distributed inertial measurement units. By establishing the coordinate transformation relationship between the local coordinate system and the reference coordinate system at any arbitrary measurement point before and after the deformation of highly flexible wings, a correlation between wing deformation and the output information from distributed inertial measurement units is established. Position and orientation information is obtained through coordinate transformation and numerical integration of the output from inertial measurement units. After obtaining the displacement and rotation angle of the measuring point, the overall displacement of the wing can be restored through interpolation.

## 2 THEORETICAL BACKGROUND

### 2.1 Differentiation of coordinate transformation matrix

Suppose there is a vector  fixed in the non-inertial system B with an angular velocity  relative to the inertial system E. According to rigid body dynamics:

$$\dot{\boldsymbol{s}}_E = \tilde{\boldsymbol{\omega}}_E \boldsymbol{s}_E \tag{1}$$

where $\tilde{\boldsymbol{\omega}}_E$ represent the skew-symmetric matrix of vector $\boldsymbol{\omega}_E$. According to the definition of coordinate transformation matrix:

$$\boldsymbol{s}_B = \boldsymbol{C}_{BE} \boldsymbol{s}_E \tag{2}$$

$$\tilde{\boldsymbol{\omega}}_B = \boldsymbol{C}_{BE} \tilde{\boldsymbol{\omega}}_E \boldsymbol{C}_{EB} \tag{3}$$

Differentiate equation (1) with respect to time, and the result is:

$$\dot{\boldsymbol{C}}_{BE} \boldsymbol{s}_E + \boldsymbol{C}_{BE} \dot{\boldsymbol{s}}_E = \dot{\boldsymbol{s}}_B = \boldsymbol{0} \tag{4}$$

From equation (1)-(4), the differential relationship between coordinate transformation matrix and angular velocity is derived:

$$\begin{cases} \dot{\boldsymbol{C}}_{BE} = -\boldsymbol{C}_{BE} \tilde{\boldsymbol{\omega}}_E = -\tilde{\boldsymbol{\omega}}_B \boldsymbol{C}_{BE} \\ \dot{\boldsymbol{C}}_{EB} = \boldsymbol{C}_{EB} \tilde{\boldsymbol{\omega}}_B = \tilde{\boldsymbol{\omega}}_E \boldsymbol{C}_{EB} \end{cases} \tag{5}$$

$$\ddot{\boldsymbol{C}}_{EB} = \dot{\boldsymbol{C}}_{EB} \tilde{\boldsymbol{\omega}}_B + \boldsymbol{C}_{EB} \dot{\tilde{\boldsymbol{\omega}}}_B \tag{6}$$

For the coordinate transformation matrix of two non-inertial system B and G, it can be calculated by multiplying two transformation matrix:

$$\boldsymbol{C}_{BG} = \boldsymbol{C}_{BE}\boldsymbol{C}_{EG} \tag{7}$$

Differentiate equation (7) with respect to time, and the result is:

$$\dot{\boldsymbol{C}}_{BG} = \dot{\boldsymbol{C}}_{BE}\boldsymbol{C}_{EG} + \boldsymbol{C}_{BE}\dot{\boldsymbol{C}}_{EG} = \boldsymbol{C}_{BG}\tilde{\boldsymbol{\omega}}_G^g - \tilde{\boldsymbol{\omega}}_B\boldsymbol{C}_{BG} \tag{8}$$

where $\boldsymbol{\omega}_G^g$ represents the angular velocity of G relative to E.

## 2.2 Position and orientation relationship

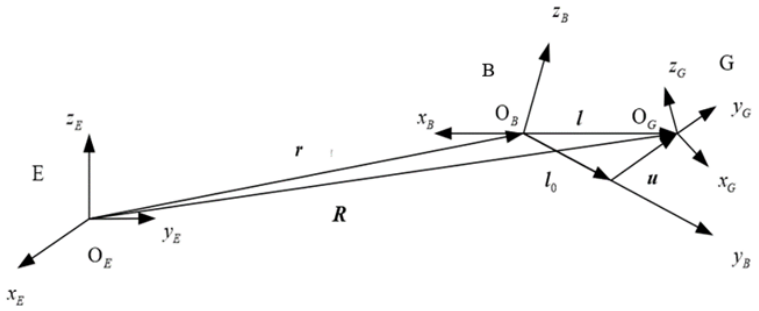


Figure 1: Position and orientation transition diagram

In Figure 1, $O_E$ represents the ground reference point, and E represents the geodetic coordinate system. $O_B$ represents the root measurement point, $O_G$ represents a certain measurement point on the wing, and B and G represent the body coordinate systems of these two IMUs, respectively. $\boldsymbol{R}$ represents the position vector from the ground reference point to the wing root measurement point, $\boldsymbol{r}$ represents the position vector from the ground reference point to the certain measurement point on the wing, $\boldsymbol{l}_0$ represents the position vector before wing deformation, $\boldsymbol{l}$ represents the position vector after wing deformation, and $\boldsymbol{u}$ represents the deformation vector.

The output of the IMU at B is: angular velocity $\boldsymbol{\omega}_B$, specific force $\boldsymbol{f}_B$ and the output of the IMU at G is: angular velocity $\boldsymbol{\omega}_G^g$, specific force $\boldsymbol{f}_G^g$. $\boldsymbol{C}_{BG}$ represent the coordinate transformation matrix from coordinate system G to coordinate system B.

Since the specific force measured by the inertial component is affected by gravitational acceleration, it is necessary to subtract the component of gravitational acceleration in the body coordinate system of the inertial component, so the actual acceleration of the measurement point is:

$$\boldsymbol{a}_B = \boldsymbol{f}_B - \boldsymbol{C}_{BE}\begin{pmatrix}0\\0\\-g\end{pmatrix} \quad \boldsymbol{a}_G^g = \boldsymbol{f}_G^g - \boldsymbol{C}_{GE}\begin{pmatrix}0\\0\\-g\end{pmatrix} \tag{9}$$

According to the geometric relationship shown in Figure 1, the relationship between the position vector, deformation vector and coordinate transformation matrix can be obtained as follows:

$$\boldsymbol{l}_B = \boldsymbol{l}_{0B} + \boldsymbol{u}_B \tag{10}$$

$$\boldsymbol{R}_E = \boldsymbol{r}_E + \boldsymbol{C}_{EB}\boldsymbol{l}_B \tag{11}$$

where $\boldsymbol{l}_{0B}$ is a constant value.

Differentiate equation (11) with respect to time, and the results are:

$$\dot{\boldsymbol{R}}_E = \dot{\boldsymbol{r}}_E + \dot{\boldsymbol{C}}_{EB}\boldsymbol{l}_B + \boldsymbol{C}_{EB}\dot{\boldsymbol{l}}_B \tag{12}$$

$$\ddot{\boldsymbol{R}}_E = \ddot{\boldsymbol{r}}_E + \ddot{\boldsymbol{C}}_{EB}\boldsymbol{l}_B + \boldsymbol{C}_{EB}\ddot{\boldsymbol{l}}_B + 2\dot{\boldsymbol{C}}_{EB}\dot{\boldsymbol{l}}_B \tag{13}$$

According to the definition of acceleration we can get $\boldsymbol{a}_E^g = \ddot{\boldsymbol{R}}_E$ and $\boldsymbol{a}_E = \ddot{\boldsymbol{r}}_E$. From equation (5)-(13), the differential equation for the deformation is derived:

$$\ddot{\boldsymbol{u}}_B + 2\tilde{\boldsymbol{\omega}}_B\dot{\boldsymbol{u}}_B + (\dot{\tilde{\boldsymbol{\omega}}}_B + \tilde{\boldsymbol{\omega}}_B\tilde{\boldsymbol{\omega}}_B)\boldsymbol{u}_B = \boldsymbol{C}_{BG}\boldsymbol{a}_G^g - \boldsymbol{a}_B - (\dot{\tilde{\boldsymbol{\omega}}}_B + \tilde{\boldsymbol{\omega}}_B\tilde{\boldsymbol{\omega}}_B)\boldsymbol{l}_{0B} \tag{14}$$

where the angular acceleration can be calculated by:

$$\dot{\tilde{\boldsymbol{\omega}}}_B = \frac{\tilde{\boldsymbol{\omega}}_B(t+\Delta t) - \tilde{\boldsymbol{\omega}}_B(t)}{\Delta t} \tag{15}$$

Once we get the acceleration and angular velocity from IMU, we can reconstruct the deformation by solving the equation (8) and (14).

### 2.3 Coordinate transformation matrix solution method

When solving the above equation, we find that the calculation accuracy of the coordinate transformation matrix greatly affects the calculation accuracy of the deformation. So a method to calcualte the coordinate transformation matrix more accurately is needed.

Equation (8) is actually a special asymmetric Liapunuov differential equation:

$$\dot{\boldsymbol{G}}(t) = \boldsymbol{A}\boldsymbol{G} + \boldsymbol{G}\boldsymbol{B}^T + \boldsymbol{D}, \quad \boldsymbol{G}(0) = \boldsymbol{G}_0 \tag{16}$$

where $\boldsymbol{G} = \boldsymbol{C}_{BG}$, $\boldsymbol{A} = -\tilde{\boldsymbol{\omega}}_B$, $\boldsymbol{B}^T = \tilde{\boldsymbol{\omega}}_G^g$ and $\boldsymbol{D} = \boldsymbol{0}$. Common numerical integration algorithms, such as Runge-Kutta, may have significant cumulative numerical errors. Zhong [11] proposed a precise integration method to numerically solve such equations, which can achieve computer accuracy. Equation (16) has a general solution:

$$\boldsymbol{G}(t) = e^{\boldsymbol{A}t}\boldsymbol{G}_0(e^{\boldsymbol{B}t})^T + \int_0^t e^{\boldsymbol{A}(t-s)}\boldsymbol{D}_0(e^{\boldsymbol{B}(t-s)})^T ds = e^{\boldsymbol{A}t}\boldsymbol{G}_0 e^{\boldsymbol{B}^T t} \tag{17}$$

Assume that the angular velocity remains constant within a time step, we have:

$$\boldsymbol{C}_{BG}(t+\Delta t)=e^{-\tilde{\boldsymbol{\omega}}_B(t)\Delta t}\boldsymbol{C}_{BG}(t)e^{\tilde{\boldsymbol{\omega}}_G^g(t)\Delta t} \tag{18}$$

The key of precise integration method is how to deal with matrix exponential. According to the addition theorem of matrix exponential functions:

$$e^{-\tilde{\boldsymbol{\omega}}_B(t)\Delta t}=(e^{\frac{-\tilde{\boldsymbol{\omega}}_B(t)\Delta t}{m}})^m,\ \ m=2^N \tag{19}$$

where $N$ is an arbitrarily chosen positive integer. $\Delta t$ is the sampling time of IMU, usually between 0.001s and 0.01s. Then $\tau=\Delta t/m$ is a very small time period, so the accuracy is sufficient to expanded the power series to five terms:

$$e^{-\tilde{\boldsymbol{\omega}}_B(t)\tau}\approx\boldsymbol{I}+(-\tilde{\boldsymbol{\omega}}_B(t)\tau)+\frac{(-\tilde{\boldsymbol{\omega}}_B(t)\tau)^2}{2!}+\frac{(-\tilde{\boldsymbol{\omega}}_B(t)\tau)^3}{3!}+\frac{(-\tilde{\boldsymbol{\omega}}_B(t)\tau)^4}{4!}=\boldsymbol{I}+\boldsymbol{T}_a \tag{20}$$

where the values of elements in $\boldsymbol{T}_a$ are very small. It will be rounded by computer when added to the identity matrix $\boldsymbol{I}$. Notice that:

$$(\boldsymbol{I}+\boldsymbol{T}_a)^{2^N}=(\boldsymbol{I}+2\boldsymbol{T}_a+\boldsymbol{T}_a^{\,2})^{2^{N-1}}=(\boldsymbol{I}+\boldsymbol{T}_{a,1})^{2^{N-1}}=\boldsymbol{I}+\boldsymbol{T}_{a,N} \tag{21}$$

After performing the operation $N$ times, $\boldsymbol{T}_{a,N}$ is no longer a small matrix. There are no serious rounding errors in this addition. $e^{\tilde{\boldsymbol{\omega}}_G^g(t)\Delta t}$ can be calculated in the same way.

## 3 NUMERICAL ANALYSIS

Taking a highly flexible flywing model as an example, this study reconstructs the wing deformation and conducts a comparative analysis with the time-domain simulation results from finite element software.

### 3.1 Model introduction

In the ABAQUS, a model of a highly flexible flywing is constructed, which is symmetrically distributed across the entire aircraft and consists of three parts: the central wing-body blending section, the two side wings, and the vertical stabilizers at the wingtips. The global coordinate system is established as shown in Figure 2, with the positive direction of the x-axis extending backward along the longitudinal axis of the fuselage, the positive direction of the z-axis pointing upward and perpendicular to the fuselage, and the positive direction of the y-axis pointing to the right wing, perpendicular to the x-z plane. The entire aircraft is modeled using B31 elements, totaling 294 elements. The finite element model of the flying wing is shown in Figure 2.

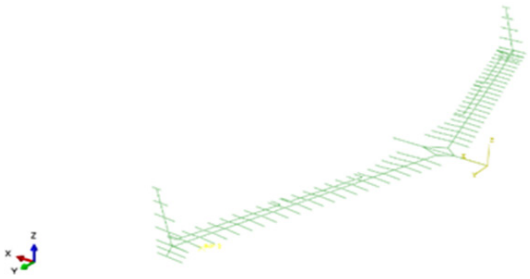

Figure 2: Highly flexible flying wing model

The main physical parameters of the flywing model are as shown in Table 1:

Table 1: Flywing model physical parameters.

| Type | Value |
|---|---|
| Semi-span length | 2.03m |
| Leading edge sweep angle | 16.5° |
| Fuselage width | 0.360m |
| Wing root (tip) chord length | 0.351(0.250)m |
| Elastic modulus | 70.0GPa |

The fuselage is fixed, and a directional dynamic load is applied at the both wings' tip: $F_x = 1\times10^3 N$, $F_z = 1.6\times10^4 N$ and the frequency is 0.5Hz.

### 3.2 Deformation reconstruction of the wingtip

Under the boundary conditions and load conditions given in 3.1, the deformation response of the wing within 60 seconds is given. The time domain simulation of ABAQUS outputs angular velocity and acceleration to simulate the measurement of inertial navigation components. Figure 3 shows the ABAQUS FEA results and reconstruction (REC) results based on the precise integration method.

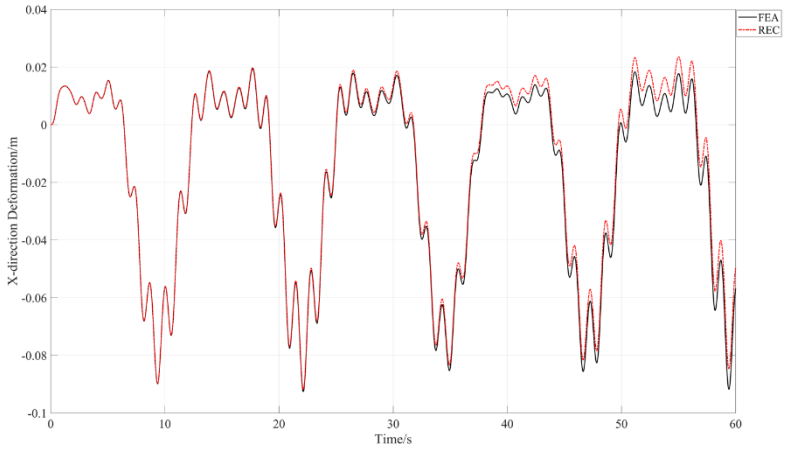


(a) X-direction deformation

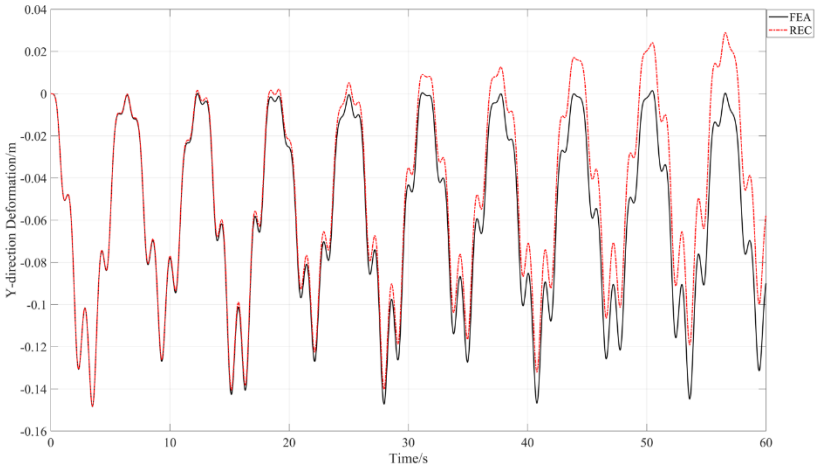


(b) Y-direction deformation

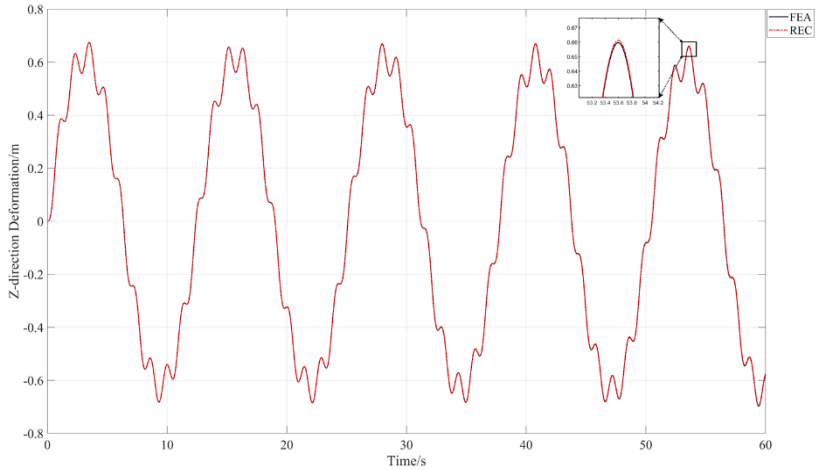


(c) Z-direction deformation

Figure 3: Wingtip deformation reconstruction

To quantitatively evaluate the accuracy of deformation reconstruction of the certain point, the error is defined as follows:

$$RMS_{local} = \frac{\left\| \boldsymbol{u}_{REC,m} - \boldsymbol{u}_{FEA,m} \right\|}{\max\left\{ \left\| \boldsymbol{u}_{FEA,m} \right\| \right\}_{m=1,2,\cdots,N}} \tag{22}$$

where $m = 1, 2, \cdots, N$ represents the number of the measurement point, $N$ represents the total number of measurement points and the denominator represents the maximum deformation of the measurement points. When m represents the point on the wingtip, the wingtip deformation error can be evaluated, which is shown in Table 2.

Table 2: Wingtip reconstruction error at certain time.

| t/s | 15 | 30 | 45 | 60 |
|---|---|---|---|---|
| $RMS_{local}$/% | 0.33 | 2.29 | 5.32 | 5.64 |

It can be seen that the reconstruction results are in good agreement with the simulation results within a certain period of time. The Z-direction (vertical) deformation curves basically coincide, while the curves in the other two directions appear to be greatly different after a long period of time. This is because the absolute value of the vertical deformation is large, while the deformation in other directions is small. By extending the simulation time, the reconstruction results will gradually deviate from the simulation results, which is due to the accumulation of errors in time-domain numerical integration in the algorithm.

From the Table 2, we can see that more samples may lead to more accurate results. However, even one sample results may achieve the highest accuracy under certain conditions. This is because the wing has different angular motion forms in different states, and using a specific function to fit it itself has a certain degree of approximation. In practical applications, the number of samples should be selected based on their motion characteristics.

### 3.3 Deformation reconstruction of the main beam

By distributed IMUs, the positions and attitudes of multiple measurement points on the wing can be obtained. Then the overall deformation of the wing can be obtained through interpolation of Euler-Bernoulli beam's shape function.

In order to study the influence of measurement points N on the accuracy of calculation results, numerical calculation results were studied for three scenarios: N=2, 4, and 6. When N=2, the measuring points are located at 42% and 92% of the total length of the main beam; when N=4, they are located at 8%, 33%, 64% and 92%; when N=6, they are located at 8%, 25%, 42%, 58%, 75% and 92%.

Figure 4 shows the deformation distribution of the wing's main beam at t=15s.

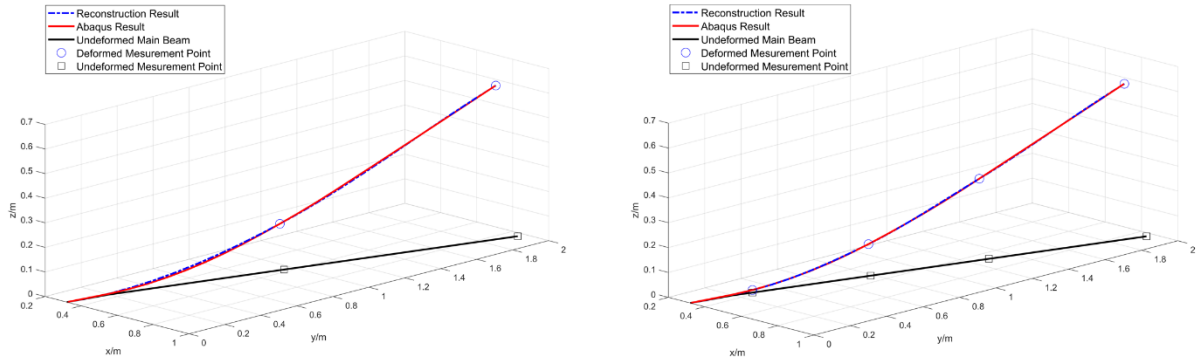


(a) 2 measurement points

(b) 4 measurement points

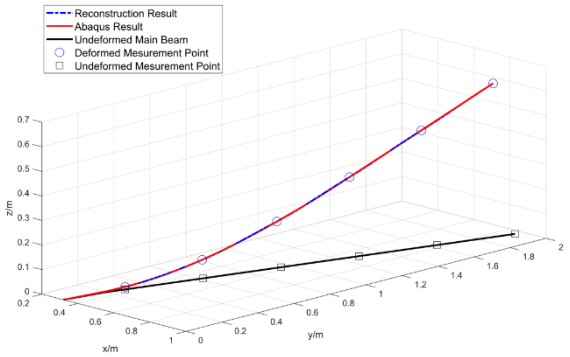


(c) 6 measurement points

Figure 4: Main beam deformation reconstruction

Table 3: Deformation of measurement points when N=2.

| $\|\boldsymbol{u}_i\|$ /m | $\|\boldsymbol{u}_1\|$ | $\|\boldsymbol{u}_2\|$ |
|---|---|---|
| FEA | 0.1951 | 0.6539 |
| REC | 0.1950 | 0.6537 |
| error | -0.05% | -0.03% |

Table 4: Deformation of measurement points when N=4.

| $\|\boldsymbol{u}_i\|$ /m | $\|\boldsymbol{u}_1\|$ | $\|\boldsymbol{u}_2\|$ | $\|\boldsymbol{u}_3\|$ | $\|\boldsymbol{u}_4\|$ |
|---|---|---|---|---|
| FEA | 0.0106 | 0.1321 | 0.3406 | 0.6539 |
| REC | 0.0105 | 0.1321 | 0.3405 | 0.6537 |
| error | -0.9% | 0% | -0.03% | -0.03% |

Table 5: Deformation of measurement points when N=6.

| $\|\boldsymbol{u}_i\|$ /m | $\|\boldsymbol{u}_1\|$ | $\|\boldsymbol{u}_2\|$ | $\|\boldsymbol{u}_3\|$ | $\|\boldsymbol{u}_4\|$ | $\|\boldsymbol{u}_5\|$ | $\|\boldsymbol{u}_6\|$ |
|---|---|---|---|---|---|---|
| FEA | 0.0106 | 0.0782 | 0.1951 | 0.3406 | 0.4966 | 0.6539 |
| REC | 0.0105 | 0.0782 | 0.1950 | 0.3405 | 0.4964 | 0.6537 |
| error | -0.9% | 0% | -0.05% | -0.03% | -0.04% | -0.03% |

where $\boldsymbol{u}_i$ is the deformation of the i-th measurement point.

To quantitatively evaluate the accuracy of deformation reconstruction of whole main beam, the root mean square error is defined as follows:

$$RMS_{global} = \sqrt{\frac{\sum_{j=1}^{nNode} \left\| \boldsymbol{u}_{REC,j} - \boldsymbol{u}_{FEA,j} \right\|^2}{\sum_{j=1}^{nNode} \left\| \boldsymbol{u}_{FEA,j} \right\|^2}} \tag{23}$$

where $j = 1, 2, \cdots, nNode$ represents the number of the interpolation nodes, and $nNode$ represents the total number of the interpolation nodes.

Table 6: Deformation RMSE of the whole main beam.

| N | $RMS_{globle}$ (%) |
|---|---|
| 2 | 9.41 |
| 4 | 3.20 |
| 6 | 2.02 |

From the Figure 4 and Table 6, it can be seen that four measurement points are sufficient to obtain relatively accurate results, and six measurement points can essentially coincide with the finite element results.

## 4 CONCLUSIONS

This paper explores the accuracy of highly flexible wing deformation reconstruction, using acceleration and angular velocity data from distributed IMUs. Time domain simulation is carried out on the flying wing model. Use the proposed method to reconstruct the deformation and verify it with the finite element simulation results. The results show that the deformation recognition accuracy within a certain period of time can meet the requirements. After a certain period of time, the accumulation error caused by the time domain numerical integration will cause the results of this algorithm to gradually deviate from the actual deformation value. The overall deformation of the main beam is reconstructed through distributed IMUs, which can achieve high reconstruction accuracy.

In the future, experiments can be conducted on actual aircraft models, and sensors without time accumulation errors can be introduced for data fusion to reduce the impact of time accumulation errors on the accuracy of deformation reconstruction.

## 5 REFERENCES

[1] Patil, M. J., Hodges, D. H. and Cesnik, C. E. S. (2004). Nonlinear aeroelastic analysis of complete aircraft in subsonic flow. *Journal of Aircraft*, 37(5): 753-760.

[2] Patil M J. (1999). *Nonlinear aeroelastic analysis flight dynamics and control of a complete aircraft*.

[3] Schneider, O. (2005). Analysis of SPR measurements from HART II. *Aerospace Science and Technology*, 9(5): 409-420.

[4] Wei, B., Liang J., Li J. and Ren M. (2017). 3D full-field wing deformation measurement method for large high-wing airplanes. *Journal of Aeronautics*, 38(07):172-181.

[5] Yuan S., Yan M., Zhang J. and Qiu L. (2014). Shape Reconstruction Method of Spar Wing Structure. *Journal of Nanjing University of Aeronautics and Astronautics*, 46(6): 825-830.

[6] Tessler, A., and Spangler, J. L. (2005). A least-squares variational method for full-field reconstruction of elastic deformations in shear-deformable plates and shells. *Computer Methods in Applied Mechanics and Engineering*, 194(2), 327–339.

[7] Lustosa, L. R., Kolmanovsky, I., Cesnik, C. E. S., and Vetrano, F. (2021). Aided Inertial Estimation of Wing Shape. *Journal of Guidance, Control, and Dynamics*, 44(2), 210–219.

[8] Srour, A. (2021). *In-Flight Wing Shape Estimation for High-Altitude Pseudo-Satellite Aircraft*.

[9] Zhang H., Liu L., Qin C., and et al. (2021). Aircraft Elastic Wing Deformation Algorithm Based on Distributed Inertial Navigation Measurement. *Journal of Beijing University of Posts and Telecommunications*, 44(06):33-39+66.

[10] Zhang W. (2010). *Research on Inertial Network System Data Fusion for Wings Flexing Estimation*.

[11] Zhong, W. and Williams, F. (1994). A Precise Time Step Integration Method. *Proceedings of the Institution of Mechanical Engineers, Part C: Journal of Mechanical Engineering Science*, 208(6), 427–430.

## COPYRIGHT STATEMENT